ACCOUNTS
of chemical research

Two-Photon Probes for Intracellular Free Metal Ions, Acidic Vesicles, And Lipid Rafts in Live Tissues

HWAN MYUNG KIM† AND BONG RAE CHO*
Department of Chemistry, Korea University, 1-Anamdong, Seoul, 136-701, Korea

RECEIVED ON AUGUST 28, 2008

Ⓦ This paper contains enhanced objects available on the Internet at http://pubs.acs.org/acr.

CONSPECTUS

Optical imaging with fluorescence microscopy is a vital tool in the study of living systems. The most common method for cell imaging, one-photon microscopy (OPM), uses a single photon of higher energy to excite the fluorophore. However, two-photon microscopy (TPM), which uses two photons of lower energy as the excitation source, is growing in popularity among biologists because of several distinct advantages. Using TPM, researchers can image intact tissue for a long period of time with minimum interference from tissue preparation artifacts, self-absorption, autofluorescence, photobleaching, and photodamage. However, to make TPM a more versatile tool in biology, researchers need a wider variety of two-photon probes for specific applications.

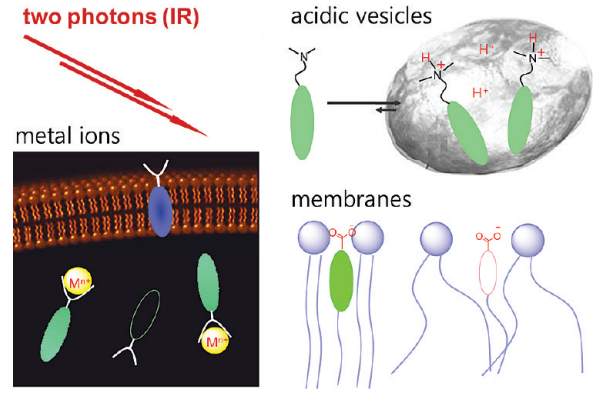

In this Account, we describe a series of two-photon probes that we developed that can visualize the distribution of intracellular metal ions, acidic vesicles, and lipid rafts in living cells and tissues. The development of these probes requires a significant two-photon cross section for the bright image and receptors (sensing moieties) that triggers the emission of the two-photon excited fluorescence upon binding with the ions or membrane in the living system. These probes also must be sensitive to the polarity of the environment to allow selective detection of cytosolic and membrane-bound probes. In addition, they need to be cell-permeable, water-soluble for the staining of cells and tissues, and highly photostable for long-term imaging.

The resulting probes—AMg1 (Mg^{2+}), ACa1−ACa3 (Ca^{2+}), AZn1 and AZn2 (Zn^{2+}), AH1, AH2, and AL1 (acidic vesicles), and CL2 (membrane)—use 2-acetyl-6-aminonaphthalene as the fluorophore and receptors for the target ions or membrane. All of these two-photon turn-on probes can detect the intracellular free metal ions, acidic vesicles, and lipid rafts at 100−300 μm depth in live tissues. Moreover, with ACa1-AM, we could simultaneously visualize the spontaneous Ca^{2+} waves in the somas of neurons and astrocytes at ~120 μm depth in fresh hypothalamic slices for more than 1000 s without appreciable decay. Furthermore, AL1 could visualize the transport of the acidic vesicles between cell body and axon terminal along the axon in fresh rat hippocampal slices at ~120 μm depth.

Introduction

Optical imaging with fluorescence microscopy is a vital tool in the study of living systems. Whereas OPM employing one photon of higher energy for the excitation is the most common method for cell imaging, TPM uses two photons of lower energy as the excitation source and is becoming more popular among biologists due to the advantages it provides. They include deeper penetration depth (>500 μm), lower tissue autofluorescence and self-absorption, and reduced photodamage and photobleaching, in addition to the intrinsically local-

Published on the Web 03/31/2009 www.pubs.acs.org/acr
10.1021/ar800185u CCC: $71.50

CHART 1. Chemical Structures of Two-Photon Probes

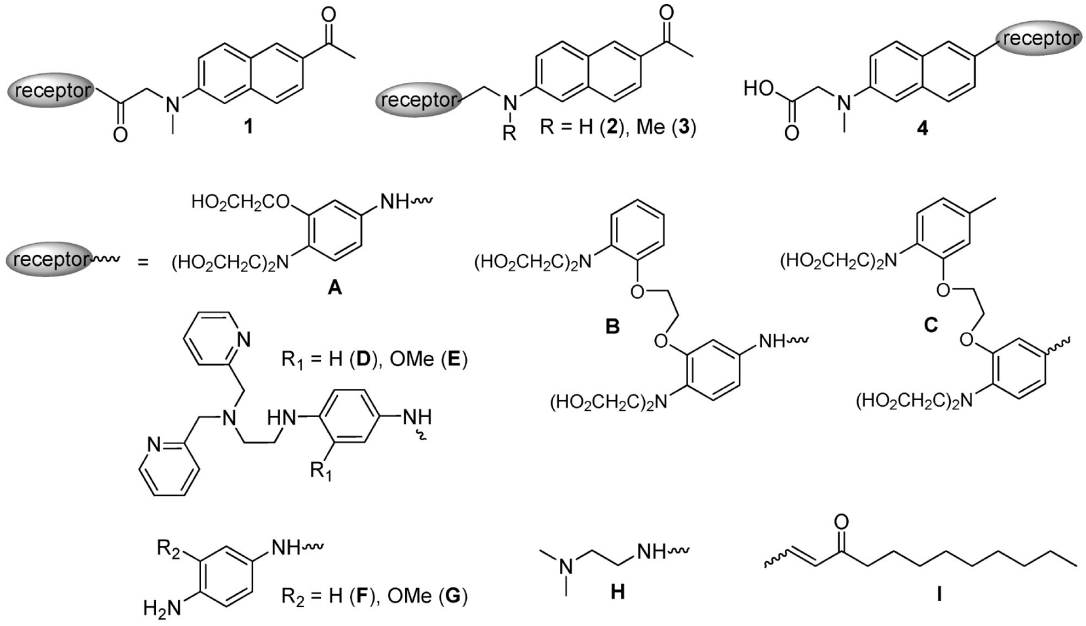

1A = **AMg1**; 1B = **ACa1**; 2C = **ACa2**; 3C = **ACa3**; 1D = **AZn1**; 1E = **AZn2**; 1F = **AH1**; 1G = **AH2**; 1H = **AL1**; 4I = **CL2**

ized excitation.[1−3] This allows imaging deep inside the intact tissue for a long period of time without the tissue preparation artifacts such as the damaged cells that can extend >70 μm into the brain slice interior.[3] However, the progress in this field is hindered by the lack of two-photon (TP) probes for specific applications. Moreover, most of the one-photon fluorescent probes used for TPM have low TP cross sections (δ_{TPA} < 50 GM) that limit their use in TPM.[4] Therefore, there is a pressing need to develop efficient TP probes with larger TP cross sections for *in vivo* imaging. This Account summarizes our design strategy, photophysical properties, and biological imaging applications of a series of TP probes for intracellular free metal ions,[5−9] acidic vesicles,[10] and biomembranes.[11−13]

Probe Design

A useful TP probe for bioimaging applications should have (i) a significant TP cross section for the bright image to obtain bright TPM images at low probe concentrations, (ii) receptors (sensing moiety) that trigger the emission of the TPEF upon binding with the ions or molecules in the living system, (iii) sensitivity to the polarity of the environment for the selective detection of cytosolic and membrane-bound probes, (iv) appreciable water solubility to stain the cells and tissues, (v) cell permeability, and (vi) high photostability for long-term imaging. We have used 6-acetyl-2-(dimethylamino)naphthalene (acedan) as the fluorophore because it was derived from 2-dodecanoyl-6-dimethylaminonaphthalene (laurdan), which is a well-known polarity-sensitive membrane probe that has been utilized in TPM imaging of the cell membrane.[14,15] Receptors were attached to the fluorophore either through a short spacer (**1**−**3**) or directly (**4**) (Chart 1).

For the turn-on probes for the cations (AMg1, ACa1−ACa3, AZn1, AZn2, AH1, AH2), receptors with higher HOMO than that of the fluorophore have been used to allow efficient PeT and quench the fluorescence. Upon binding with a cation, the probe will emit fluorescence because PeT is not possible (Figure 1a). Moreover, due to the high sensitivity of the fluorophore to the polarity of the environment, the emission resulting from the probe−cation complexes in the cytosol would be selectively detected from that of the membrane-bound probes by using different detection windows (Figure 1a). TP probes for the acidic vesicles (AL1) and lipid rafts (CL2) have been designed to emit TPEF only in the respective domains (Figure 1b,c). To improve water solubility and cell

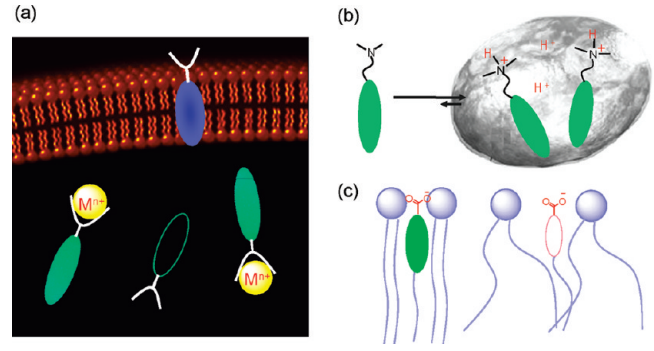

FIGURE 1. Design of two-photon turn-on probes for (a) cations, (b) acidic vesicles, and (c) biomembranes.

TABLE 1. Photophysical Data for the Two-Photon Probes

target	probe	solvent	$\lambda_{max}^{(1)}/\lambda_{max}^{fl}$ [a]	Φ [b]	K_d^{QP}/K_d^{TPc}	FEF/TFEF [d]	$\lambda_{max}^{(2)}$ [e]	δ [f]	$\Phi\delta$ [g]
Mg^{2+}	AMg1	H_2O [h]	365/498	0.58	1.4/1.6 mM	16/17	780	215	125
	ACa1	H_2O [i]	365/498	0.49	0.27/0.25 μM	40/44	780	230	110
Ca^{2+}	ACa2	H_2O [i]	362/495	0.42	0.14/0.16 μM	42/50	780	210	90
	ACa3	H_2O [i]	375/517	0.38	0.13/0.14 μM	25/23	780	250	95
Zn^{2+}	AZn1	H_2O [j]	365/498	0.47	1.1/1.1 nM	21/24	780	210	86
	AZn2	H_2O [j]	365/499	0.65	0.5/0.5 nM	54/52	780	140	95
Acidic vesicles	AH1	H_2O [k]	364/498	0.60	4.4/4.5 [l]	22/26	780	140	86
	AH2	H_2O [k]	365/496	0.64	4.5/4.5 [l]	64/68	780	138	88
	AL1	H_2O [k]	364/496	0.72	*m*	*m*	780	130	92
Lipid Rafts	CL2	DMF	392/535	0.51	*m*	*m*	800	230	120
		EtOH	401/580	0.09	*m*	*m*	800	250	20

[a] λ_{max} of the one-photon absorption and emission spectra in nanometers. [b] Fluorescence quantum yield. [c] Dissociation constants measured by one- (K_d^{QP}) and two-photon (K_d^{TP}) processes, except otherwise noted. [d] Fluorescence enhancement factor, $(F - F_{min})/F_{min}$, measured by one- (FEF) and two-photon (TFEF) processes. [e] λ_{max} of the two-photon excitation spectra in nanometers. [f] The peak two-photon cross section in 10^{-50} cm^4 s/photon (GM). [g] Two-photon action cross section. [h] Tris buffer (100 mM KCl, 20 mM NaCl, 1 mM EGTA, pH 7.05), 10 mM, in the presence of 50 mM free Mg^{2+}. [i] MOPS buffer (100 mM KCl, 10 mM EGTA, pH 7.2), 30 mM, in the presence of 39 μM free Ca^{2+}. [j] MOPS buffer, 30 mM, in the presence of 1.8 μM free Zn^{2+}. [k] Universal buffer (0.1 M citric acid, 0.1 M KH_2PO_4, 0.1 M $Na_2B_4O_7$, 0.1 M Tris, 0.1 M KCl, pH 3.2). [l] pK_a values determined by one- and two-photon processes. [m] Not applicable.

permeability, hydrogen-bonding sites were introduced and the molecular weights were kept as low as possible. All compounds show TP action cross section on the order of 100 GM presumably because of the efficient intramolecular charge transfer and high quantum yield.[5−10] It is well established that the TP cross section increases with the extent of intramolecular charge transfer, and dipolar molecules with similar molecular weight have been shown to exhibit similar TP cross sections to that of acedan.[16] Photophysical properties of the TP probes are summarized in Table 1.

Two-Photon Probe for Magnesium Ion

Magnesium ion plays crucial roles in many cellular processes such as cell proliferation and cell death, enzymatic reactions, and signal transduction.[17,18] To detect its distribution throughout living systems, we have developed a TP fluorescent probe (AMg1) having acedan as the fluorophore and *o*-aminophenol-*N*,*N*,*O*-triacetic acid (APTRA) as the Mg^{2+}-selective binding site (Chart 1).[6]

AMg1 is a TP turn-on probe with TP fluorescence enhancement factor (TFEF) of 17 in Tris buffer solution (10 mM, pH 7.05). The K_d^{QP} values of AMg1 for Mg^{2+} and Ca^{2+} ions are 1.4 ± 0.1 mM and 9.0 ± 0.3 μM, respectively, which are very similar to those measured for the TP processes (Table 1). AMg1 showed modest to strong response toward Mg^{2+}, Ca^{2+}, Zn^{2+} and Mn^{2+}, and much weaker response toward Fe^{2+}, Cu^{2+}, and Co^{2+}. The intracellular Mg^{2+} ion concentration (0.1−6.0 mM) is much higher than that of Ca^{2+} (10 nM to 1 μM),[19] so that this probe can detect intracellular free Mg^{2+} in the millimolar range without interference by other metal ions. Moreover, AMg1 and AMg1−Mg^{2+} were pH-insensitive in the biologically relevant pH range. The TP action cross section of AMg1−Mg^{2+} complex is 125 GM at 780 nm, which is 7-fold larger than those of MgG−Mg^{2+} and Mag-fura-2−Mg^{2+}.[19] This indicates that TPM images would be much brighter when stained with AMg1 than with the commercial probes.

The TPM image of AMg1-AM-labeled Hep3B cells revealed intense (red) spots and homogeneous (green) domains (Figure 2a). The TPEF spectra of the two regions could be fitted to two Gaussian functions centered at 439 and 488 nm (sky blue) and at 426 and 498 nm (brown), respectively (Figure 2d). The peak positions of the dissected spectra were similar, suggesting that the probes might be located in two regions with different polarity. Moreover, the excited-state lifetime of the intense spots was 3.3 ns, which was longer than the upper extreme in the lifetime distribution curve (Figure S1, Supporting Information). From these results, we hypothesized that the probes might be located in two different environments, a more polar one that is likely to be cytosol, which gives red emission with a shorter lifetime, and a less polar one that is likely to be membrane-associated, which emits blue light with an extended lifetime. To provide supporting evidence for this hypothesis, we have studied the effect of carbonyl cyanide *m*-chlorophenylhydrazone (CCCP), which prevents ATP-Mg^{2+} production from ADP, inorganic phosphate, and Mg^{2+} by uncoupling oxidative phosphorylation and thereby increases the intracellular free Mg^{2+} concentration.[20] When CCCP was added to Hep3B cells labeled with AMg1-AM, the TPEF intensity in the 500−620 nm region increased immediately after addition and then decreased to the baseline level (Figure 2e). In contrast, no change in the TPEF intensity was noted in the 360−460 nm range, indicating that it is indeed from the AMg1-AM located in the cell membrane. Therefore, one can selectively detect the intracellular AMg1−Mg^{2+} complexes with minimal interference due to the membrane bound probes by using the detection window at 500−620 nm. It is to be noted that membrane-associated Mg^{2+} ions play an impor-

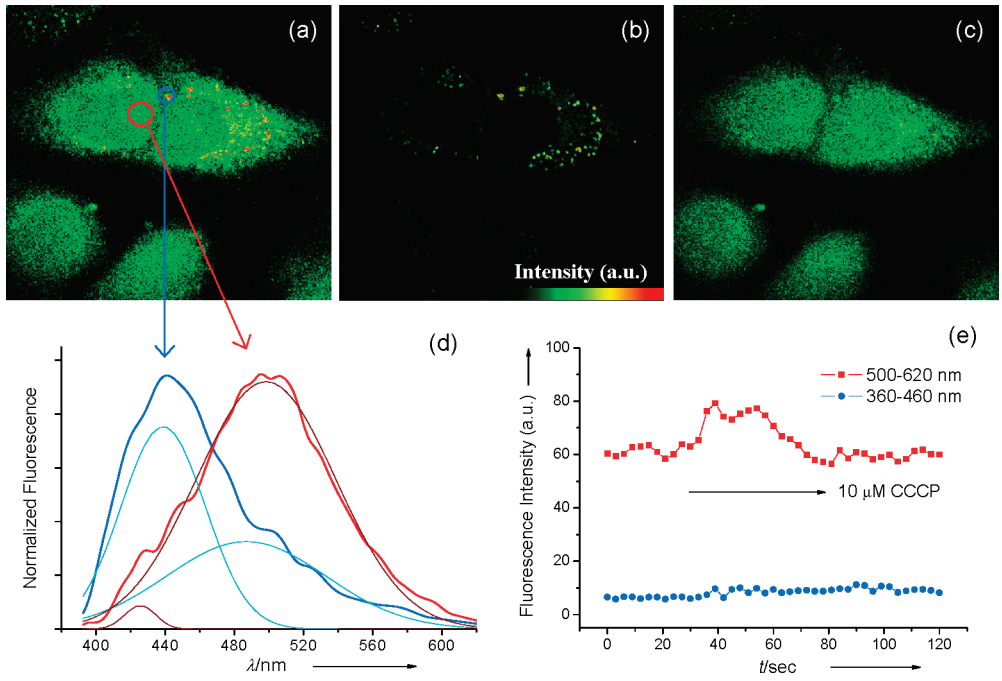

FIGURE 2. TPM images collected at 360−620 (a), 360−460 (b), and 500−620 nm (c) of AMg1-AM-labeled (2 μM) Hep3B cells. (d) Two-photon excited fluorescence spectra from the hydrophobic (blue) and hydrophilic (red) domains of AMg1-AM-labeled Hep3B cells. The excitation wavelength is 780 nm. Cells shown are representative images from replicate experiments. (e) TPEF intensity collected at 500−620 (red) and 360−460 nm (blue) before and after addition of CCCP as a function of time.

tant role in the regulation of protein synthesis, as illustrated in the magnesium membrane mitosis (MMM) model.[17] Indeed, the TPEF image collected at 500−620 nm is homogeneous without the red spots, whereas the latter can be clearly seen in the images collected at 360−460 nm (Figure 2b,c).

The TPM image of fresh hippocampal slices from postnatal 3-day mice labeled with 5 μM AMg1-AM revealed intracellular free Mg^{2+} distribution in the CA1 and CA3 regions as well as in the dentate gyrus at ~270 μm depth (Figure 3b). Moreover, the images taken at higher magnifications resolved intracellular free Mg^{2+} distribution in the pyramidal neuron layer of the CA1 region (Figure 3c,d). Furthermore, a closer examination of Figure 3d revealed that this probe could also detect the Mg^{2+} ions in the nucleus in the tissue. These results demonstrate that AMg1 is capable of detecting endogenous stores of labile Mg^{2+} at 100−300 μm depth in live tissues using TPM.

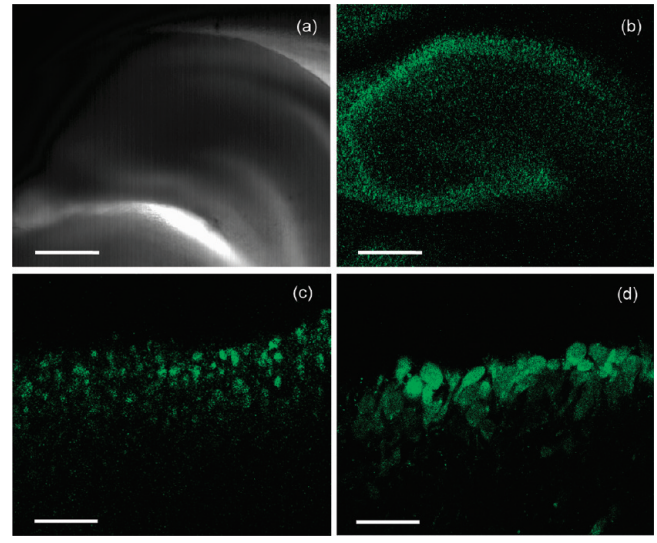

FIGURE 3. Images of a fresh mouse hippocampal slice stained with 5 μM AMg1-AM: (a) bright-field image shows the CA1 and CA3 regions as well as the dentate gyrus by magnification at 10×; (b) TPM image with the same magnification reveals the same regions at a depth of ~270 μm; (c) magnification at 40× shows the CA1 layer at a depth of ~150 μm; (d) magnification at 100× shows CA1 pyramidal neurons at a depth of ~150 μm. Scale bars = 300 (a, b), 120 (c), and 30 (d) μm. The TPEF images were collected at 500−620 nm upon excitation at 780 nm with femtosecond pulses.

Two-Photon Fluorescent Probes for Calcium Ion

Calcium is a ubiquitous intracellular messenger, it is an essential regulator of many cellular processes including fertilization, cell death, sensory transduction, muscle contraction, motility, exocytosis, and fluid secretion.[21,22] Calcium triggers exocytosis within microseconds and drives gene transcription and proliferation in minutes to hours. The concentration varies from 100 nM at rest to 1 μM upon activation.[21,22] To understand these functions, we have developed a series of TP probes (ACa1−ACa3) that can visualize the calcium waves

deep inside live tissue without photobleaching or mistargeting problems (Chart 1).[7,8]

ACa1−ACa3 are TP turn-on probes with TFEF values ranging from 25 to 42.[8] The K_d^{TP} values of ACa1−ACa3 for Ca^{2+} are in the range of 0.14−0.25 μM, indicating that they can detect Ca^{2+} in the submicromolar range (Table 1). ACa1−ACa3 showed modest response toward Zn^{2+} and Mn^{2+}, much weaker response toward Mg^{2+}, Fe^{2+} and Co^{2+}, no response toward Cu^{2+}, and were pH-insensitive in the biologically relevant pH range. Because of the negligible intracellular concentrations of free Mn^{2+}, these probes can selectively detect the intracellular free Ca^{2+} concentration in the regions where the chelatable Zn^{2+} concentration is much lower than K_d^{TP} for Ca^{2+}. Furthermore, the $\Phi\delta_{max}$ values of the probe−Ca^{2+} complexes in buffer solutions were 90−110 GM at 780 nm, approximately 4-fold larger than that of OG1−Ca^{2+}.[19] Accordingly, the TPM image of ROS17/2.8 cells was much brighter when labeled with ACa1-AM than with OG1-AM (Figure S2, Supporting Information). Hence, the intracellular free Ca^{2+} could be detected by TPM utilizing these probes with minimal errors due to the membrane-bound probes and other metal ions by using the detection window at 500−620 nm.

To demonstrate the utility of these probes, we have monitored calcium waves in live cells and tissue. The TPM images of cultured astrocytes labeled with 2 μM ACa1-AM revealed a spontaneous Ca^{2+} wave propagation from the astrocytic process (1) to soma (2) to terminal (3) with a speed of 7.5 ± 2.2 μm/s (Figure S3 and video of Figure S3, Supporting Information), indicating that the signal propagates in the same direction. The calcium wave also propagated between astrocytes at a slower rate (1.8 ± 1.1 μm/s). Thus it is evident that ACa1 is clearly capable of visualizing the intra- and intercellular calcium waves in cultured astrocytes using TPM.[7]

The TPM images of individual astrocytes in fresh hypothalamic slices from the postnatal 1-day rat labeled with 10 μM ACa1-AM revealed the spontaneous calcium waves in the soma (Figure 4, trace 1) for more than 1100 s without appreciable decay (see video of TPEF images). Furthermore, the spikes at the astrocyte process (Figure 4, trace 2) appeared slightly before those in the soma (trace 1), confirming the above finding that the signals propagate from the process to the soma. A similar result was observed with ACa2-AM, except that the observation time was 4000 s.[8] In contrast, OPM images of the tetrodotoxin (TTX) treated thalamus slice stained with fura-2[23] revealed damaged cells on the tissue surface and was not as clear as the TPM image presented here. Also, the fluorescence intensity decayed appreciably after 500 s.[23] The improved TPM image of ACa2-labeled tissue obtained at

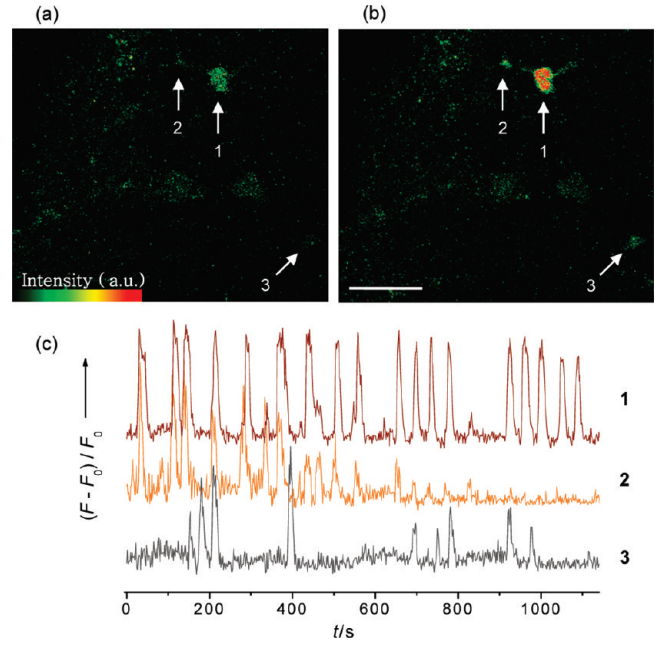

FIGURE 4. Pseudocolored TPM images of a fresh rat hypothalamic slice stained with 10 μM ACa1-AM taken after 195 (a) and 214 (b) s. Magnification at 100× shows hypothalamic area at a depth of ~170 μM. (c) Spontaneous Ca^{2+} transients recorded in soma (1), astrocyte process (2), and neighboring cell (3). The TPEF images were collected at 500−620 nm upon excitation at 780 nm with femtosecond pulses. Scale bar, 30 μm.

Ⓦ A video file of the TPEF images in mp4 format is available.

~120 μm depth for a prolonged observation time underlines the high photostability and low phototoxicity of this probe in addition to its capability of deep tissue imaging.

Two-Photon Fluorescent Probes for Zinc Ion

Zinc ion is a vital component of enzymes and proteins.[24,25] In the brain, a few millimoles of intracellular free Zn^{2+} is stored in the presynaptic vesicles, released with synaptic activation, and seems to modulate excitatory neurotransmission.[25] To visualize the intracellular free Zn^{2+} ion distribution inside the live tissue, we have developed TP probes (AZn1 and AZn2) derived from acedan as the fluorophore and *N*,*N*-di-(2-picolyl)ethylenediamine (DPEN) as the Zn^{2+} chelator (Chart 1).[9]

AZn1 and AZn2 are TP turn-on probes with TFEF of 21 and 54, respectively. The larger TFEF for AZn2 has been attributed to the *o*-MeO group, which has reduced Φ of the probe by facilitating PeT and enhanced Φ of the probe−Zn^{2+} complex by inducing a tighter binding between the probe and Zn^{2+}.[9] The K_d^{TP} values for AZn1 and AZn2 were 1.1 ± 0.1 and 0.50 ± 0.04 nM, respectively. The smaller K_d^{TP} for AZn2 is consistent with the tighter binding between the probe and Zn^{2+}. Both probes showed high selectivity for Zn^{2+} and were pH-

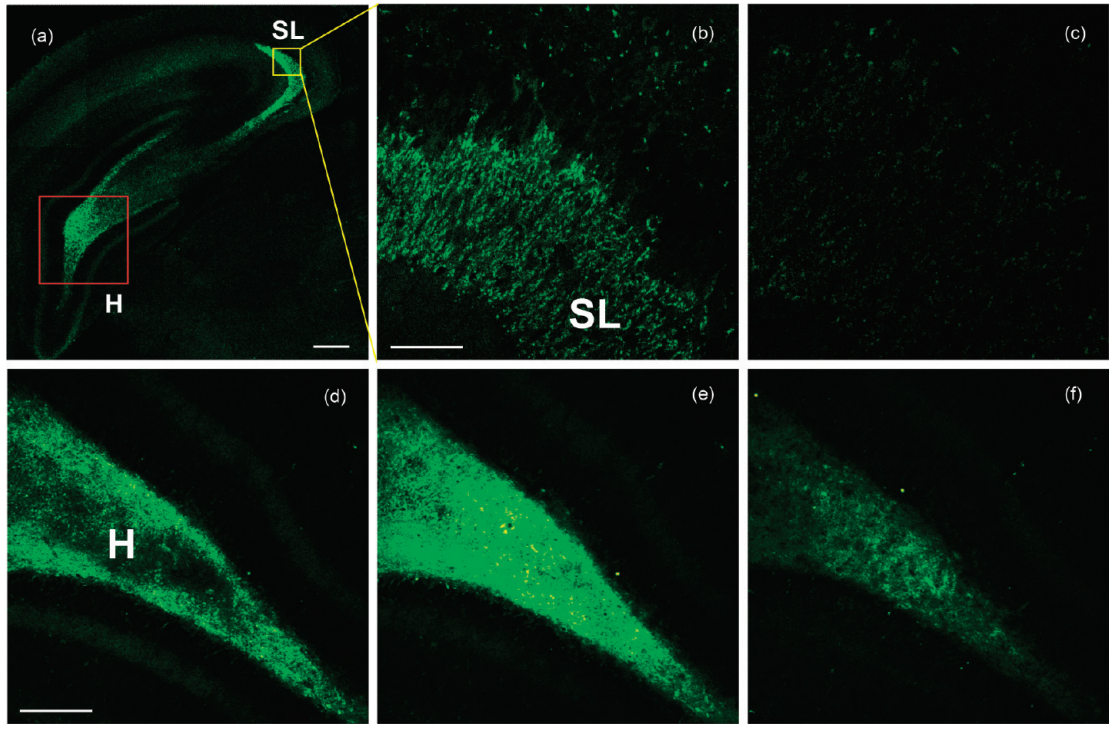

FIGURE 5. TPM images of a rat hippocampal slice stained with 10 μM AZn2: (a) TPM image at a depth of ~120 μm with magnification 10×. Scale bar, 300 μm. (b, c) Magnification at 100× in stratum lucidum (SL) of CA3 regions (yellow box) at a depth of ~100 μm (b) before and (c) after addition of 200 μM TPEN to the imaging solution. Scale bar, 150 μm. (d–f) TPM images in the hilus (H) of dentate gyrus (DG) regions at a depth of ~100 μm (d) before and (e) after addition of 50 mM KCl to the imaging solution. (f) After addition of 200 μM TPEN to tissue from panel e. Scale bar, 300 μm. The TPEF images were collected at 500–620 nm upon excitation at 780 nm with femtosecond pulse.

insensitive in the biologically relevant pH. The TP action spectra of the Zn^{2+} complexes with AZn1 and AZn2 in buffer solutions indicated a $\Phi\delta$ value of ~90 GM at 780 nm, 4–24-fold larger than those of TSQ and FluZin-3;[19] TPM images for samples stained with AZn1 and AZn2 would be much brighter than those stained with commercial probes.

The TPM images of 293 cells labeled with both probes emitted no TPEF at 360–460 nm, and appreciable TPEF at 500–620 nm (Figure S4, Supporting Information). They appear to be predominantly located in the cytosolic compartments, probably due to the appreciable water solubility, and thereby can detect the intracellular Zn^{2+} in live cells without interference from membrane-bound probes. When 10 mM *S*-nitrosocysteine (SNOC), an endogenous NO donor that triggers the release of Zn^{2+}, was added to the cell, the TPEF intensity increased gradually with time and then decreased abruptly upon addition of 0.1 mM *N*,*N*,*N*′,*N*′-tetrakis(2-pyridyl)-ethylenediamine (TPEN), a membrane-permeable Zn^{2+} chelator that can effectively remove Zn^{2+}.[26] A similar result was observed with AZn1 except that the response was smaller, understandably due to the larger K_d. Hence, these probes are clearly capable of detecting the intracellular free Zn^{2+} in live cells.

To investigate the utility of this probe in tissue imaging, TPM images were obtained from a part of fresh rat hippocampal slice incubated with 10 μM AZn2 for 30 min at 37 °C. Because the slice of a 14-day old rat was too big to show with one image, several TPM images were obtained in the same plane at ~120 μm depth and combined. It reveals intense fluorescence in the stratum lucidum (SL) of CA3 and the hilus (H) of dentate gyrus (DG) (Figure 5a).[27] The image obtained at a higher magnification clearly shows that intracellular free Zn^{2+} is concentrated in the mossy fiber axon terminals of pyramidal neurons in the CA3 region (Figure 5b). The negligible TPEF after addition of TPEN provides supporting evidence for this observation (Figure 5c). When 50 mM KCl, a membrane depolarizer causing the release of Zn^{2+}, was added to the imaging solution, the TPEF intensity increased and then decreased upon treatment with TPEN (Figure 5d–f). These findings demonstrate that AZn2 is capable of detecting intracellular free Zn^{2+} at 80–150 μm depth in live tissues using TPM.

Two-Photon Fluorescent Probes for Acidic Vesicles

Lysosomes and lysosome-related organelles constitute a system of acidic compartments (pH 4.0–5.0), which contain a

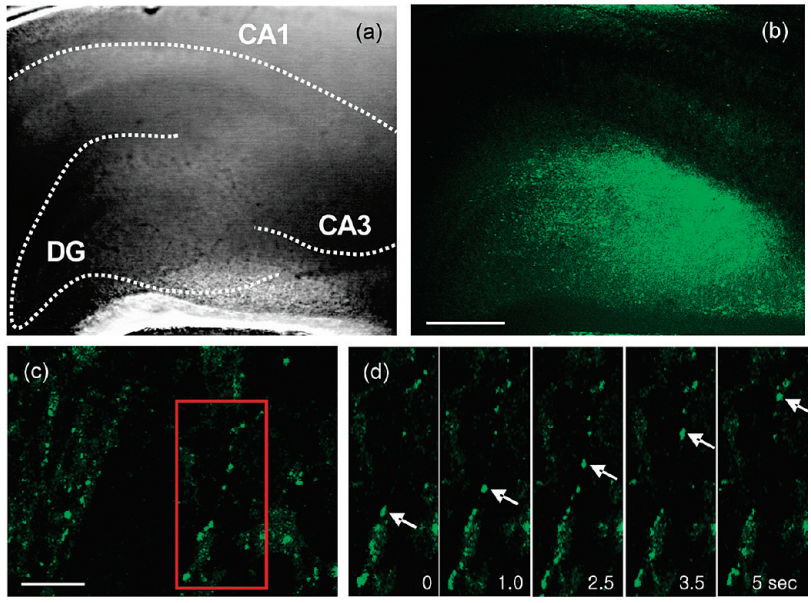

FIGURE 6. Images of a fresh rat hippocampal slice stained with 10 μM AL1. (a) Bright field image shows the CA1 and CA3 regions as well as the dentate gyrus (DG) upon magnification 10×. White dotted lines indicate the pyramidal neuron layer. (b) Forty TPM images were accumulated along the *z*-direction at the depth of ~100−250 μm with magnification 10× to visualize the average distribution of the acidic vesicles in the same regions. (c) Magnification 100× in CA3 regions at a depth of ~120 μm. (d) Enlargement of a red box in panel c shows the transport of acidic vesicles along the axon. Scale bars, 300 (b) and 30 (c) μm.

Ⓦ A video of the transport of acidic vesicles along the axon in mp4 format is available.

large number of enzymes and secretory proteins exhibiting a variety of functions.[28,29] To visualize their distribution in live tissues, we have developed acedan-derived TP pH probes (AH1, AH2) and a TP lysotracker (AL1) (Chart 1).[10] We have introduced aniline and *o*-methoxyaniline [pK_a(BH$^+$) ≈ 4] or a tertiary amine [pK_a(BH$^+$) ≈ 10] as the proton binding site via the amide linkage to the acedan fluorophore with an expectation that AH1 and AH2 would emit TPEF upon protonation at pH < 4, and AL1 emits TPEF in the acidic vesicles where it can be accumulated as the protonated form (Figure 1b).[19]

AH1 and AH2 are TP turn-on probes for the acidic vesicles with the TFEF of 26 and 68, respectively. The larger TFEF for AH2 has been attributed to the 3-fold decrease in Φ from AH1 (Φ = 0.03) to AH2 (Φ = 0.01) at pH 7.0 due to the *o*-OMe group (*vide supra*). Moreover, the pK_a values of the conjugate acids of AH1 and AH2 estimated from the fluorescence titration curves are 4.42 ± 0.03 and 4.48 ± 0.02, respectively, indicating that they are suitable for detecting acidic vesicles with pH < 4. On the other hand, there was little change in the fluorescence spectra of AL1 with the pH change. The TP action cross section of AH1, AH2, and AL1 at pH 3.2 was ~90 GM at 780 nm, 9-fold larger than that of LysoTracker Red (LTR);[19] TPM images of the samples stained with these probes would be much brighter than those stained with LTR.

To demonstrate the utility of these probes, TPM images were obtained of individual macrophages labeled with 2 μM AH1, AH2, and AL1. The TPM images of AH2- and AL1-labeled macrophages emitted TPEF only at 500−620 nm and not at 360−460 nm (Figure S5, Supporting Information). Moreover, the TPEF spectra of the intense and bright spots in the TPM images of the AH2-labeled cells were almost the same as that of AH2 in the buffer solution with λ^{fl}_{max} of ~500 nm.[10] A nearly identical result was observed in the TPM images of AH2- and AL1-labeled tissues.[10] These results suggest that the probes are predominantly located in the hydrophilic regions in the cell, presumably because of the appreciable water solubility. To unambiguously determine the utility of these probes, the macrophages were costained with AH2 and LTR, a well-known one-photon fluorescent probe for the acidic vesicles,[19] and the TPM image was colocalized with the OPM image. The two images were well merged (Figure S5, Supporting Information), confirming that both probes can detect acidic vesicles. Similar results were obtained in the colocalization experiments of AL1 and AH1 with LTR. Hence, these probes are clearly capable of imaging the acidic vesicles in live cells by TPM.

We further investigated the utility of AL1 and AH2 in tissue imaging. The bright field image of a part of fresh rat hippocampal slice from the postnatal 2-day rat labeled with 10

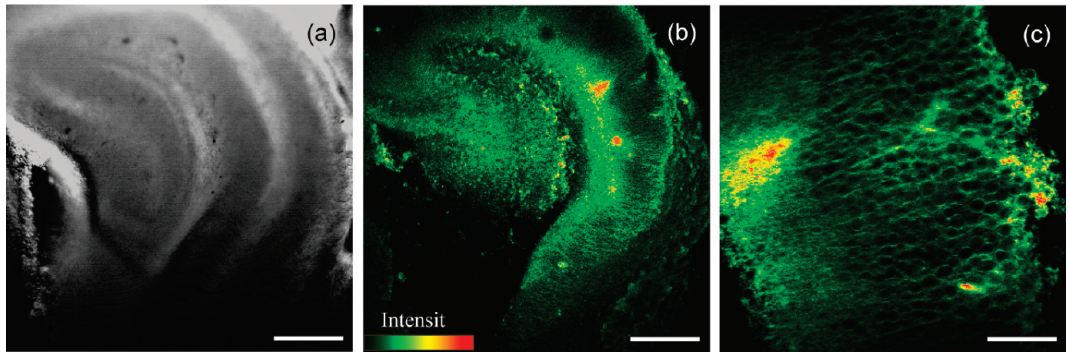

FIGURE 7. Images of a fresh rat hippocampal slice stained with 10 μM CL2. (a) Bright-field image of the CA1 and CA3 regions, as well as the dentate gyrus, by 10× magnification. (b) TPM image of the CA1 and CA3 regions by 10× magnification. Twenty-five TPM images were accumulated along the *z*-direction at the depth of ~100−250 μm. (c) TPM image of the CA1 layer at a depth of ~120 μm by 40× magnification. The TPM images were collected at 410−530 nm upon excitation at 800 nm with femtoseconds pulses. Scale bars, 300 (a,b) and 75 (c) μm.

μM AL1 (or AH2) reveals the CA1 and CA3 regions as well as the dentate gyrus (DG) (Figure 6a). The TPM images reproduced by accumulating 40 TPM images obtained at different depth in the range of 100−250 μm show that the acidic vesicles are more abundant in CA3 and DG than in CA1 region (Figure 6b). Moreover, the real time images reveal rapid transportation of the acidic vesicles between the cell body and axon terminal along the axon (Figure 6c,d, and video of transport of acidic vesicles along the axon).[30] Furthermore, the activity of the acidic vesicles could be visualized for more than 1100 s without appreciable decay.[10] This underlines the high photostability of this probe in addition to the capability of deep tissue imaging. Finally, AL1 was found to be superior to AH2 in monitoring the vesicle transportation, although both are capable of detecting the acidic vesicles deep inside the live tissues.

Two-Photon Probes for Biomembrane

The lipid rafts hypothesis proposes that plasma membrane has rigid compartments [liquid-ordered (l_o) phase] enriched with glycosphingolipids and cholesterol floating in the sea of glycerophospholipids [liquid-disordered (l_d) phase].[31−33] The rigid compartments, also called rafts, are believed to be involved in many cellular processes such as signal transduction, pathogen invasion, cholesterol homeostasis, neurodegenerative diseases, and angiogenesis.[31−33] However, the existence of such a domain in biological membranes is controversial.[34]

Membrane lateral heterogeneity in the cells has most often been studied by GP images of laurdan-labeled cells with TPM.[14,15] However, the literature results based on laurdan are hard to reproduce, presumably because of negligible water solubility. To overcome this problem, we have developed 6-dodecanoyl-2-[*N*-methyl-*N*-(carboxymethyl)-amino]naphthalene (CL), which shows the advantages of greater sensitivity to the polarity, brighter two-photon fluorescence images, and more accurate reflection of the cell environment than laurdan.[11,12] The major drawback of the polarity probes such as laurdan and CL is that their function relies on the GP value, which may lead to a significant experimental error.[11,35] A solution to this problem would be to design a turn-on probe that emits TPEF exclusively in the domains of lipid rafts. To address the above needs, we have designed 6-[(*E*)-3-oxo-1-dodecenyl]-2-[*N*-methyl-*N*-(carboxymethyl)amino]naphthalene (CL2) possessing a longer conjugation length to enhance the TP cross section for a brighter TPM image and to increase the sensitivity of the fluorescence intensity relative to its environment polarity for the selective detection of the lipid rafts in live cells and tissues without invoking the GP values (Chart 1).[13]

CL2 showed sufficient water solubility to stain the cells, high sensitivity to the solvent polarity, dramatic decrease in the fluorescence intensity with the polarity of the solvents and vesicles, higher preference to reside in the l_o than in the l_d domain, and a large TP cross section (250 GM in EtOH).[13] Moreover, the TP action cross section ($\Phi\delta_{max}$) of CL2 is 8-fold larger in 1,2-dipalmitoyl-*sn*-glycero-3-phosphocholine (DPPC) than in 1,2-dioleoyl-*sn*-glycero-3-phosphocholine (DOPC), due to the more hydrophobic environment of DPPC and high preference of CL2 to reside in the l_o domain. This allows the direct visualization of the l_o domain against the dim background due to the l_d domain by TPM. Furthermore, CL2 showed much higher photostability in DPPC ($t_{1/2}$ = 2100 s) than in DOPC ($t_{1/2}$ = 60 s), and visualizing the lipid rafts for a long period of time is feasible.

The TPM images of the CL2-labeled giant unilamellar vesicles composed of raft mixture, a good model for the biomembrane, revealed intense and dim domains that can be

attributed to the existence of discrete l_o-like and l_d-like domains.[13] Moreover, the TPM image of CL2-labeled macrophages showed bright regions (red color), which disappeared upon treatment with methyl-β-cyclodextrin (MβCD), a lipid raft destroying reagent, and returned to near normal upon treatment with cholesterol (Figure S6, Supporting Information).[35] To determine unambiguously whether the red-colored domains are indeed the lipid rafts, the macrophages were costained with CL2 and BODIPY-G_{M1}, a well-known one-photon fluorescence probe for the lipid raft,[36] and the TPM image was colocalized with the one-photon fluorescence image. Bright regions on the two images were well overlapped, confirming that the bright regions reflect lipid rafts (Figure S6, Supporting Information).

To demonstrate the utility of this probe in tissue imaging, fresh hippocampal slices from postnatal 3-day mice were incubated with 10 μM CL2 for 30 min at 37 °C. The bright field image of a part of fresh mouse hippocampal slice reveals the CA1 and CA3 regions as well as the dentate gyrus (Figure 7a). The TPM images revealed that lipid rafts are more abundant in the radiatum layer composed of axon bundles than in the pyramidal neuron layer composed of cell bodies (Figure 7b). Moreover, the images taken at higher magnifications resolved the distribution of lipid rafts in the pyramidal neuron layer of the CA1 region (Figure 7c).

Conclusions

We have developed a series of TP probes that can visualize the distribution of intracellular metal ions, acidic vesicles, and lipid rafts in live cells and tissues. The probes for the cytosolic metal ions and acidic vesicles should exhibit appreciable water solubility to stain the samples, significant TP action cross section for the bright TPM image, receptors that trigger the TPEF emission upon binding with target ions or vesicles, sensitivity to the polarity of the environment for the selective detection of the target ions or vesicles without interference from the membrane bound probes, and high photostability for long-time imaging. For the turn-on probes, the HOMO of the receptor should be higher than that of the fluorophore to make the PeT more efficient. The membrane probes should have similar properties as mentioned above except that they emit TPEF in different wavelength range depending on the membrane polarity or in l_o domain only. Water solubility can be improved by introducing hydrogen-bonding sites and photostability by incorporating conjugation bridges within the cycle. To increase the TP action cross section without detrimental effects on water solubility and cell permeability, the molecular size has to be optimized. Therefore, the right combination of the fluorophore, receptor, and linker between them is crucial for the designing of a useful TP probe.

This work was supported by the Korea Science and Engineering Foundation grant funded by the Korea Ministry of Education, Science, and Technology (No. R0A-2007-000-20027-0).

Supporting Information Available. Supporting Figures S1−S6 and video (mp4 format) of Figure S3. This material is available free of charge via the Internet at http://pubs.acs.org.

BIOGRAPHICAL INFORMATION

Hwan Myung Kim received his B.S. in Chemistry from Chung Nam National University. He joined Prof. Cho's group at Korea University and received his Ph.D. in 2008. He is a full time lecturer in the Department of Chemistry at Ajou University.

Bong Rae Cho graduated from Seoul National University with a B.S. in Chemistry and received his Ph.D. from Texas Tech University. He is a Professor of Chemistry at Korea University.

ABBREVIATIONS

OPM	one-photon microscopy
TP	two-photon
TPM	two-photon microscopy
TPEF	two-photon excited fluorescence
GM	Göppert−Mayer, unit of two-photon absorption in 10^{-50} cm^4 s/photon
$\Phi\delta_{max}$	peak two-photon action cross section, a measure of the peak two-photon excited fluorescence intensity in GM
PeT	photoinduced electron transfer
GP	generalized polarization, GP = $(I_o - I_d)/(I_o + I_d)$, where I_o and I_d are the fluorescence intensities in the liquid-ordered and liquid-disordered domains, respectively

FOOTNOTES

* Corresponding author. Mailing address: Molecular Opto-Electronics Laboratory, Department of Chemistry, Korea University, 1-Anamdong, Seoul, 136-701, Korea. Tel: +82-2-3290-3129. Fax: +82-2-3290-3544. E-mail: chobr@korea.ac.kr.

† Present address: Department of Chemistry, Ajou University, Suwon 443-749, Korea.

REFERENCES

1 Zipfel, W. R.; Williams, R. M.; Webb, W. W. Nonlinear magic: Multiphoton microscopy in the biosciences. *Nat. Biotechnol.* **2003**, *21*, 1369–1377.

2 Helmchen, F.; Denk, W. Deep tissue two-photon microscopy. *Nat. Methods* **2005**, *2*, 932–940.

3 Williams, R. M.; Zipfel, W. R.; Webb, W. W. Multiphoton microscopy in biological research. *Curr. Opin. Chem. Biol.* **2001**, *5*, 603–608.

4 Xu, C.; Zipfel, W.; Shear, J. B.; Williams, R. M.; Webb, W. W. Multiphoton fluorescence excitation: New spectral windows for biological nonlinear microscopy. *Proc. Natl. Acad. Sci. U.S.A.* **1996**, *93*, 10763–10768.

5 Kim, H. M.; Yang, P. R.; Seo, M. S.; Yi, J. S.; Hong, J. H.; Jeon, S. J.; Ko, Y. G.; Lee, K. J.; Cho, B. R. Magnesium ion selective two-photon fluorescent probe based on a benzo[h]chromene derivative for in vivo imaging. *J. Org. Chem.* **2007**, *72*, 2088–2096.

6 Kim, H. M.; Jung, C.; Kim, B. R.; Jung, S. Y.; Hong, J. H.; Ko, Y. G.; Lee, K. J.; Cho, B. R. Environment-sensitive two-photon probe for intracellular free magnesium ions in live tissue. *Angew. Chem., Int. Ed.* **2007**, *46*, 3460–3463.

7 Kim, H. M.; Kim, B. R.; Hong, J. H.; Park, J. S.; Lee, K. J.; Cho, B. R. A two-photon fluorescent probe for calcium waves in living tissue. *Angew. Chem., Int. Ed.* **2007**, *46*, 7445–7448.

8 Kim, H. M.; Kim, B. R.; An, M. J.; Hong, J. H.; Lee, K. J.; Cho, B. R. Two-photon fluorescent probes for long-term imaging of calcium waves in live tissue. *Chem.—Eur. J.* **2008**, *14*, 2075–2083.

9 Kim, H. M.; Seo, M. S.; An, M. J.; Hong, J. H.; Tian, Y. S.; Choi, J. H.; Kwon, O.; Lee, K. J.; Cho, B. R. Two-photon fluorescent probes for intracellular free zinc ions in living tissue. *Angew. Chem., Int. Ed.* **2008**, *47*, 5167–5170.

10 Kim, H. M.; An, M. J.; Hong, J. H.; Jeong, B. H.; Kwon, O.; Hyon, J. Y.; Hong, S. C.; Lee, K. J.; Cho, B. R. Two-photon fluorescent probes for acidic vesicles in live cells and tissue. *Angew. Chem., Int. Ed.* **2008**, *47*, 2231–2234.

11 Kim, H. M.; Choo, H. J.; Jung, S. Y.; Ko, Y. G.; Park, W. H.; Jeon, S. J.; Kim, C. H.; Joo, T.; Cho, B. R. A two-photon fluorescent probe for lipid raft imaging: C-laurdan. *ChemBioChem* **2007**, *8*, 553–559.

12 Kim, H. M.; Kim, B. R.; Choo, H. J.; Ko, Y. G.; Jeon, S. J.; Kim, C. H.; Joo, T.; Cho, B. R. Two-photon fluorescent probe for biomembrane imaging: Effect of chain length. *ChemBioChem* **2008**, *9*, 2830–2838.

13 Kim, H. M.; Jeong, B. H.; Hyon, J. Y.; An, M. J.; Seo, M. S.; Hong, J. H.; Lee, K. J.; Kim, C. H.; Joo, T.; Hong, S. C.; Cho, B. R. Two-photon fluorescent turn-on probe for lipid rafts in live cell and tissue. *J. Am. Chem. Soc.* **2008**, *130*, 4246–4247.

14 Gaus, K.; Gratton, E.; Kable, E. P.; Jones, A. S.; Gelissen, I.; Kritharides, L.; Jessup, W. Visualizing lipid structure and raft domains in living cells with two-photon microscopy. *Proc. Natl. Acad. Sci. U.S.A.* **2003**, *100*, 15554–15559.

15 Sanchez, S. A.; Gratton, E. Lipid-protein interactions revealed by two-photon microscopy and fluorescence correlation spectroscopy. *Acc. Chem. Res.* **2005**, *38*, 469–477.

16 Kim, H. M.; Cho, B. R. Two-photon materials with large two-photon cross sections. Structure−property relationship. *Chem. Commun.* **2009**, 153−164. 10.1039/b813280a.

17 Rubin, H. Magnesium: The missing element in molecular views of cell proliferation.

18 *Magnesium and the Cell*; Birch, N. J., Ed.; Academic Press: San Diego, CA, 1993.

19 *The Handbooks-A Guide to Fluorescent Probes and Labeling Techonologies*, 10th ed.; Haugland, R. P. Ed.; Molecular Probes: Eungene, OR, 2005.

20 Nelson, D. L.; Cox, M.; Lehninger M., *Principles of Biochemistry*, 4th ed.; W. H. Freeman & Company: New York, 2005; p 707.

21 Berridge, M. J.; Bootman, M. D.; Roderick, H. L. Calcium signalling: Dynamics, homeostasis and remodeling. *Nat. Rev. Mol. Cell. Biol.* **2003**, *4*, 517–529.

22 Rizzuto, R.; Pozzan, T. Microdomains of intracellular Ca^{2+}: Molecular determinants and functional consequences. *Physiol. Rev.* **2006**, *86*, 369–408.

23 Parri, H. R.; Gould, T. M.; Crunelli, V. Spontaneous astrocytic Ca^{2+} oscillations in situ drive NMDAR-mediated neuronal excitation. *Nat. Neurosci.* **2001**, *4*, 803–812.

24 Vallee, B. L.; Falchuk, K. H. The biochemical basis of zinc physiology. *Physiol. Rev.* **1993**, *73*, 79–118.

25 Frederickson, C. J.; Koh, J. Y.; Bush, A. I. The neurobiology of zinc in health and disease. *Nat. Rev. Neurosci.* **2005**, *6*, 449–462.

26 Chang, C. J.; Jaworski, J.; Nolan, E. M.; Sheng, M.; Lippard, S. J. A tautomeric zinc sensor for ratiometric fluorescence imaging: Application to nitric oxide-induced release of intracellular zinc. *Proc. Natl. Acad. Sci. U.S.A.* **2004**, *101*, 1129–1134.

27 Koh, J. Y.; Suh, S. W.; Gwag, B. J.; He, Y. Y.; Hsu, C. Y.; Choi, D. W. The role of zinc in selective neuronal death after transient global cerebral ischemia. *Science* **1996**, *272*, 1013–1016.

28 Blott, E. J.; Griffiths, G. M. Secretory lysosomes. *Nat. Rev. Mol. Cell. Biol.* **2002**, *3*, 122–131.

29 Stinchcombe, J.; Bossi, G.; Griffiths, G. M. Linking albinism and immunity: The secrets of secretory lysosomes. *Science* **2004**, *305*, 55–59.

30 Hartman, K. N.; Pal, S. K.; Burrone, J.; Murthy, V. N. Activity-dependent regulation of inhibitory synaptic transmission in hippocampal neurons. *Nat. Neurosci.* **2006**, *9*, 642–649.

31 Simons, K.; Toomre, D. Lipid rafts and signal transduction. *Nat. Rev. Mol. Cell. Biol.* **2000**, *1*, 31–9.

32 Munro, S. Lipid rafts: Elusive or illusive. *Cell* **2003**, *115*, 377–388.

33 Anderson, R. G.; Jacobson, K. A role for lipid shells in targeting proteins to caveolae, rafts, and other lipid domains. *Science* **2002**, *296*, 1821–1825.

34 Jacobson, K.; Mouritsen, O. G.; Anderson, R. G. Lipid rafts: At a crossroad between cell biology and physics. *Nat. Cell Biol.* **2007**, *9*, 7–14.

35 Furuchi, T.; Anderson, R. G. Cholesterol depletion of caveolae causes hyperactivation of extracellular signal-related kinase (ERK). *J. Biol. Chem.* **1998**, *273*, 21099–21104.

36 Janes, P. W.; Ley, S. C.; Magee, A. I. Aggregation of lipid rafts accompanies signaling via the T cell antigen receptor. *J. Cell. Biol.* **1999**, *147*, 447–461.